ELSEVIER

International Journal of Mass Spectrometry 179/180 (1998) 77–90

International Journal of Mass Spectrometry

Exploring the potential energy surfaces of the reactions of $O^+(^4S)$ and $O^+(^2D)$ with ammonia

Ana I. González, Otilia Mó, Manuel Yáñez*

Departamento de Química, C-9, Universidad Autónoma de Madrid, Cantoblanco, 28049-Madrid, Spain

Received March 19, 1998; accepted May 27, 1998

Abstract

High-level ab initio calculations in the framework of the G2 and CBS-Q theories have been performed for the $[H_3,N,O]^+$ doublet and quartet state cations. The geometries of the different stationary points of both potential energy surfaces (PESs) were optimized at the QCISD/6-31+G(df,p) level. The bonding characteristics of doublet and quartet state cations are rather different. The latter are weakly bound species involving one-electron linkages, while the former present normal covalent bonds. The global minimum of the doublet PES is the HO-NH_2^+ **2D** species, which has a N–O linkage with a partial double-bond character. This means that the ionization of hydroxylamine implies an important enhancement of the stability of the N–O bond, which upon ionization becomes much shorter, although its stretching frequency is significantly blue-shifted. For the quartets the global minimum can be viewed roughly as the interaction between O in its ^3P ground state and NH_3^+. From the characteristics of both $[H_3,N,O]^+$ doublet and quartet state potential energy surfaces we conclude that the products of $O^+(^rS)$ and $O^+(^2D)$ reactions with ammonia are significantly different. For reactions involving O^+ in its ^4S ground state, only the charge transfer process should be observed, in agreement with the experimental evidence. In reactions involving O^+ in its ^2D first excited state, the charge transfer process is energetically disfavored with respect to H and H_2 loss. Hence, the major product ions should be H_2NO^+, HNO^+, NOH^+, $HNOH^+$ and in a much smaller proportion NH_3^+, $NH_2^+(^1A_1)$, and $NH^+(^2\Pi)$. The exothermicity of H_3^+ reactions with NO to yield NOH^+, HNO^+, and H_2NO^+ (which may be important depletion mechanisms for NO in the interstellar clouds) is also discussed. (Int J Mass Spectrom 179/180 (1998) 77–90) © 1998 Elsevier Science B.V.

Keywords: High-level ab initio calculations; $O^+ + NH_3$ reactions; Potential energy surfaces

1. Introduction

The role of cation-molecule reactions in atmospheric and interstellar chemistry has made this area one of the most attractive and interesting fields within gas-phase ion chemistry [1]. The contributions of Cacace and co-workers to this development are very significant. It is worth mentioning, for instance, that Cacace and Speranza reported [2], only a few years ago, the first experimental determination of the proton affinity of ozone. The reader is also addressed to a nice overview of the future of this field recently published by Cacace [3].

The availability of high-level ab initio molecular orbital techniques also contributed to this develop-

* Corresponding author.

Dedicated to Professor Fulvio Cacace on the occasion of his 40th anniversary in the field of gas-phase ion chemistry and physics.

PII S1387-3806(98)14062-9

ment. Actually, due to the difficulties that an experimental study of these kind of reactions presents, their theoretical treatment has become crucial in gaining understanding of the thermodynamic properties and structures of the systems involved in them. On one hand, ab initio techniques currently allow the prediction of properties of neutral and charged species within ± 1 kcal/mol: the so-called chemical accuracy. On the other hand, they are, in many cases, the only alternative available to investigate the structures of ionic species, which quite often are elusive to experimental observation. Even when such techniques are amenable to the experiment, the rationalization of the empirical evidences usually requires a good knowledge of the most outstanding characteristics of the corresponding potential energy surface (PES), which, only in very few cases, can be obtained or deduced experimentally. Ab initio calculations also provide useful information with respect to the harmonic vibrational frequencies, allowing the estimation of important thermodynamic properties like the magnitude of the zero point energy (ZPE) corrections or the changes in the entropy along the reactive process.

Our research group has carried out in recent years detailed studies on several cation-molecule systems, paying special attention to those processes that involve open-shell monocations such as C^+ [4], Si^+ [5,6], F^+ [7], Cl^+ [8], etc. Very recently we have reported the stationary points of $[H_2, O_2]^+$ PESs either when the multiplicity of the system is doublet or quartet [9]. These PESs can be associated with the reaction of O^+, either in its ^4S ground state or in its ^2D first excited state with water. In this study we provide evidence for the necessity of including high order contributions to the correlation energy, through the use of the QCISD method [10], to adequately describe the geometries of weakly bound open-shell cations, like the $[H_2,O_2]^+$ quartets. A similar conclusion was reported very recently by Mayer et al. [11] for the treatment of radicals.

Our aim in this work is to perform a similar study on the system $[H_3,N,O]^+$. In this case we can associate the ionic species investigated with the reaction between $O^+(^4S)$ or $O^+(^2D)$ with NH_3, which is one of the most abundant interstellar inorganic molecules. Also, interestingly, one of the minimum of the doublet PES corresponds to the ionization of hydroxylamine, an interesting and well-known molecule, whose gas-phase reactivity toward electrophiles was investigated by Cacace and co-workers [12].

We will focus our attention on the comparison of the structures, bonding characteristics, and relative stabilities of $[H_3,N,O]^+$ doublet- and quartet-state cations and on the most outstanding features of the corresponding PESs.

2. Computational details

Correlation effects are important when describing structural features, but they are usually crucial for open-shell species [13]. Hence, the geometries of the systems investigated were initially optimized at the MP2(full)/6-31G* level. Since the PES around weakly bound species is usually very flat, these geometry optimizations were performed using tight convergency criteria. The harmonic vibrational frequencies were evaluated at the same level in order to classify the stationary points found as minima or transition states and to estimate the ZPE corrections. As we have shown previously for the particular case of $[H_2,O_2]^+$ quartet-state cations [9], electron correlation effects have special relevance as far as the structures of open-shell weakly bound species are concerned. Furthermore, they are particularly sensitive to high order correlation corrections as well as to the inclusion of diffuse and high angular momentum functions in the basis set. Taking this into account we have refined the aforementioned MP2 geometries of all the stationary points found at the QCISD/6-31+G(df,p) level. In all cases we have also systematically checked the stability of the corresponding wavefunctions. In this respect, it must be mentioned that only for the less stable $[H_3,N,O]^+$ quartet-state cations were some instabilities detected. In these cases a stabilization of the wavefunction was carried out using the techniques currently available in the GAUSSIAN 94 series of programs [14]. We have also checked, taking the most stable quartet cation as a suitable example, that the aforementioned QCISD

optimized geometry does not change significantly when a more costly CCSD approach is used (see Fig. 1).

To obtain the corresponding final energies of the species under investigation we have used two different high-level ab initio techniques, namely the G2 theory of Pople et al. [15] and the CBS-Q formalism of Petersson et al. [16] which usually provide thermodynamic properties as heats of formation, protonation energies, ionization potentials, etc., within chemical accuracy. The G2 approach is a composite procedure which yields final energies of an effectively QCISD(T)/6-311+G(3df,2p) quality. It must be noted that, although the geometries used in the standard G2 procedure are optimized at the MP2(full)/6-31G* level and the ZPE corrections are evaluated at the HF/6-31G* level, in the present case we have used the QCISD/6-31+G(df,p) optimized geometries, whereas the ZPE corrections were evaluated at the MP2/6-31G* level and scaled by the empirical factor 0.9646 [17]. The results so obtained will be denoted hereafter as G2//QCI.

The CBS-Q formalism [16] extrapolates correlation energies from finite pair natural orbital expansions in order to estimate the results that would be obtained from complete basis set calculations. The full CI limit is estimated through the use of the QCISD(T) procedure and the basis sets employed range from the small 6-31G†† basis to the very large (14s9p4d2f,6s3p1d)/[6s6p3d2f,4s3p1d] atomic pair natural orbital basis set. Although the standard CBS-Q calculations are based on MP2 optimized geometries (as in the G2 calculations) in our case we have used the QCISD/6-31+G(df,p) optimized ones. The results so obtained will be denoted hereafter as CBS-Q//QCI.

The bonding characteristics of the different local minima were analyzed by means of two different partition techniques, namely, the natural bond orbital (NBO) analysis of Weinhold et al. [18] and the atoms in molecules (AIM) theory of Bader [19]. The first technique permits a description of the different bonds of the system in terms of the natural hybrid orbitals centered on each atom and also provides useful information on the charge distribution of the system. The AIM formalism is based on a topological analysis of the electron charge density, $\rho(\mathbf{r})$ and its Laplacian, $\nabla^2\rho(\mathbf{r})$. More specifically, we have located the so-called bond critical points, i.e. points where $\rho(\mathbf{r})$ is minimum along the bond path and maximum in the other two directions. In general, the values of ρ and $\nabla^2\rho$ at these points provide useful information on the bonding characteristics. In most cases negative values of the Laplacian are associated with covalent linkages, while positive values are usually associated with closed-shell interactions like those found in ionic bonds, van der Waals complexes, and hydrogen bonds. More reliable for this purpose is the energy density, H(**r**), in the sense that negative values of H(**r**) are always associated with covalent linkages [20] even in those particular cases (as with the F_2 molecule) where the Laplacian is positive. Since, as mentioned above, electron correlation effects are crucial for the systems under study, both population analyses were performed at the QCISD level. AIM calculations have been carried out by using the AIMPAC series of programs [21].

3. Results and discussion

3.1. Structures, bonding characteristics, and relative stabilities

The QCISD/6-31+G(df,p) optimized structures of $[H_3,N,O]^+$ doublet- and quartet-state cations are given schematically in Fig. 1. The different species are identified by a number followed by **D** or **Q** to distinguish between doublet- and quartet-state cations, respectively. Their G2//QCI and CBS-Q//QCI total energies are summarized in Table 1. This table also includes the $\langle S^2\rangle$ expectation values to show that, with the only exception of the two transition states involved in the loss of H, the contamination of the unrestricted wavefunction is very small. This low spin contamination [11] and the fact that the energy gap between the highest occupied and the lowest empty molecular orbitals (MOs) is reasonably large, allowed us to assume [22] that the species investigated are adequately described by single determinant based approaches.

It can be observed that although the CBS-Q total energies are systematically lower than the correspond-

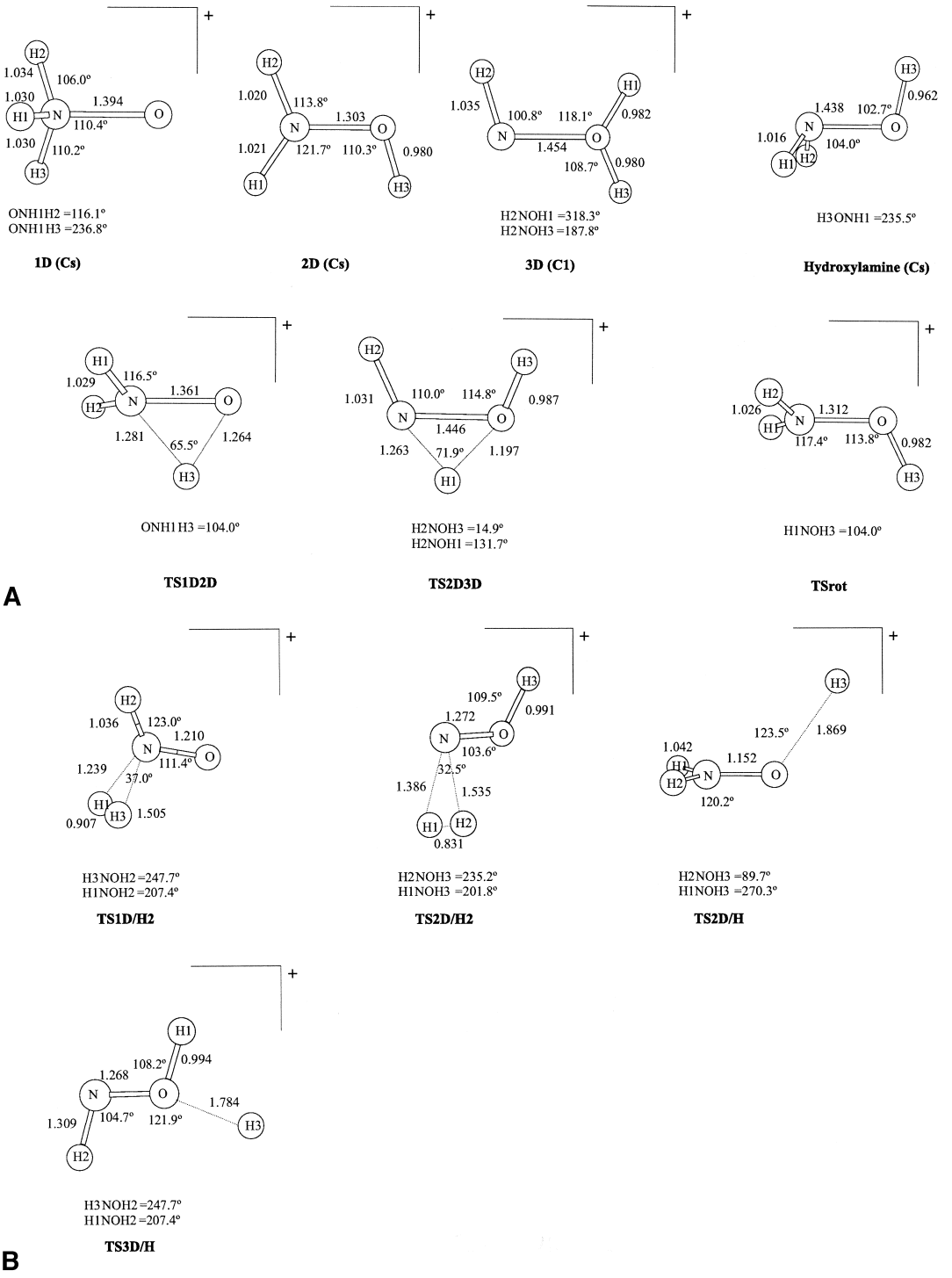

Figure 1 (*continued on next page*)

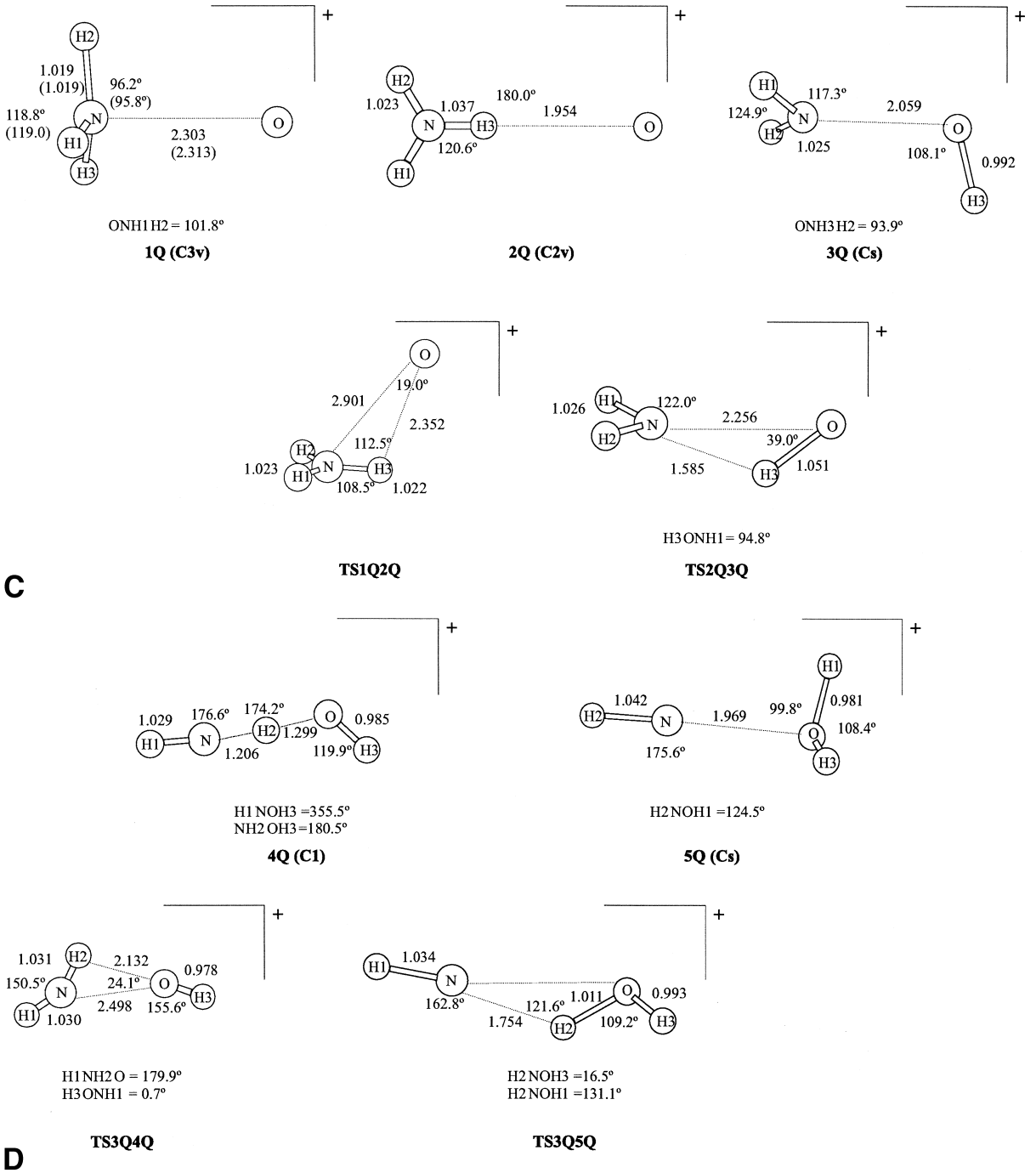

Fig. 1 (*continued from previous page*). QCISD/6-31+G(df,p) optimized geometries of the stationary points of the $[H_3,N,O]^+$ doublet- and quartet-state cations. Bond lengths are in Å. Bond and dihedral angles are in degrees. For the most stable quartet-state cation **1Q**, the values within parentheses were obtained in CCSD/6-31+G(df,p) geometry optimization.

Table 1
Total energies in hartrees. Values within parentheses are relative stabilities (in kJ/mol) with respect to **2D** and **1Q**, respectively. All relative energies include MP2/6-31G* ZPE corrections scaled by the empirical factor 0.9646

	E(G2//QCISD/6-31+G(df,p))	E(CBS-Q//QCISD/6-31+G(df,p))	$\langle S^2 \rangle$
1D	−131.157115 (94)	−131.163904 (94)	0.759
2D	−131.192784[a] (0.0)	−131.199947 (0.0)	0.767
3D	−131.136736 (147)	−131.142700 (150)	0.760
TS1D2D	−131.099631 (245)	−131.107393 (243)	0.810
TS2D3D	−131.082086 (291)	−131.089020 (291)	0.767
TS1D/H2	−131.05700 (356)		0.796
TS2D/H2	−131.048652 (378)		0.765
TS2D/H	−131.076506[a] (305)		0.976
TS3D/H	−131.042055[a] (395)		1.039
TSrot	−131.173070 (52)		0.763
1Q	−131.076041 (0.0)	−131.082332 (0.0)	3.775
2Q	−131.075150 (3)	−131.080546 (5)	3.778
3Q	−131.049483 (70)	−131.057340 (66)	3.789
4Q	−131.058844 (45)	−131.064673 (46)	3.778
5Q	−131.061853 (37)	−131.070123 (32)	3.779
TS1Q2Q	−131.064233 (31)	−131.070037 (32)	3.768
TS1Q3Q	−131.026999 (129)	−131.035304 (123)	3.777
TS3Q4Q	−131.041005 (92)	−131.047894 (90)	3.778
TS3Q5Q	−131.044552 (83)	−131.047893 (82)	3.775
Hydroxylamine	−131.533377		0.0

[a]The CCSD(T)/6-311+G(3df,2p)//QCISD/6-31+G(df,p) total energies for these species, including ZPE corrections, are: −131.161248, −131.044615, and −131.010070 hartrees, respectively. The corresponding relative energies are identical to those obtained at the G2//QCISD/6-31+G(df,p) level.

ing G2 values, the relative energies are rather similar. It is worth noting, however, that these differences are slightly higher for quartets than for doublets. This is likely due to the fact that (as it has been found for other weakly bound open shell cations) electron correlation effects are quite important; and whereas in the G2 formalism the full CI limit is estimated in QCISD(T) type calculations using 6-311G(d,p) basis set expansions, in the CBS-Q approach the smaller 6-31G†† basis is used. The fact that both methods provide similar results is in agreement with the conclusion of Mayer et al. [11], in the sense that when the spin contamination is low, as in our case, the G2 theory performs adequately.

The first conspicuous feature of Fig. 1 is that doublets and quartets present significantly different bonding characteristics. This is quite apparent when considering, for instance, species **1D** and **1Q**. Both result from the attachment of O^+ to the nitrogen of the NH_3 molecule and exhibit N–O distances which differ by almost 1 Å. This is consistent with the fact that although for the doublet-state cation the Laplacian within the N–O bonding region is negative (−0.445 a.u.), as in typical covalent bonds, in the quartet it is positive (+0.132 a.u.), indicating that the interaction is essentially electrostatic. As we shall discuss later in more detail, all quartet-state cations can be classified as weakly bound species, while the doublets are covalently bound structures.

3.2. $[H_3,N,O]^+$ doublet potential energy surface

There are sizable differences in the bonding characteristics of the different doublet-state cations, which are clearly reflected in their optimized geometries and in the values of the charge densities and energy densities at the corresponding bond critical points (see Table 2), and which will be reflected in their relative stabilities.

In Fig. 2, we have plotted schematically the most significant features of the doublet PES. The attachment of $O^+(^2D)$ to the nitrogen atom of ammonia would yield the **1D** local minimum. Taking into account that $O^+(^2D)$ has a very large electron recombination energy (16.6 eV) [23], the first step would imply a charge transfer from the neutral (which has a much smaller ionization potential, 10.18eV [15]) to the cation, yielding $O + NH_3^+$. The second step

Table 2
Characteristics of the N–O bonds. Charge densities, $\rho(\mathbf{r})$, and energy densities, $H(\mathbf{r})$ at the bond critical points, are in atomic units

	$\rho(\mathbf{r})$	$H(\mathbf{r})$
1D	0.335	−0.329
2D	0.393	−0.468
3D	0.269	−0.228
1Q	0.038	0.004
3Q	0.065	0.003
5Q	0.075	0.001
Hydroxylamine	0.293	−0.266

would be the formation of a covalent linkage between one of the unpaired electrons of the oxygen atom and the unpaired electron of the $NH_3^{\cdot +}$ subunit. The result is the formation of a distonic **1D** cation, where the unpaired electron is located on the oxygen atom, although the positive charge is essentially associated with the NH_3 moiety. Once the **1D** species is formed, a 1,2H shift (through the transient species **TS1D2D**) yields species **2D**, which exhibits a stronger N–O bond because this 1,2H shift reinforces the π-bonding interactions, as illustrated in Fig. 3. In the left part of this figure we have plotted the schematic representations of the π-type occupied molecular orbitals of species **1D** which correlate, in the right of the figure, with the MOs of species **2D**. It can be seen that *a* and *b* are N–O bonding MOs, whereas *c* and *d* are N–O antibonding in both species. The first important change induced by the 1,2H shift is that the two hydrogen atoms that remain attached to the nitrogen and the one attached to the oxygen atom become coplanar in order to reinforce the bonding interactions of the former with the N orbitals in both *a* and *c* MOs. As a consequence, the contribution of the hydrogen orbitals to *b* and *d* MOs becomes null (see Fig. 3), because in species **2D** these π-MOs are perpendicular to the plane that contains the hydrogen atoms, and their N–O bonding and N–O antibonding character changes significantly. However, these effects do not cancel each other because orbital *b* is doubly occupied whereas orbital *d* is singly occupied. Hence, a net increase in the bonding character takes place, and the

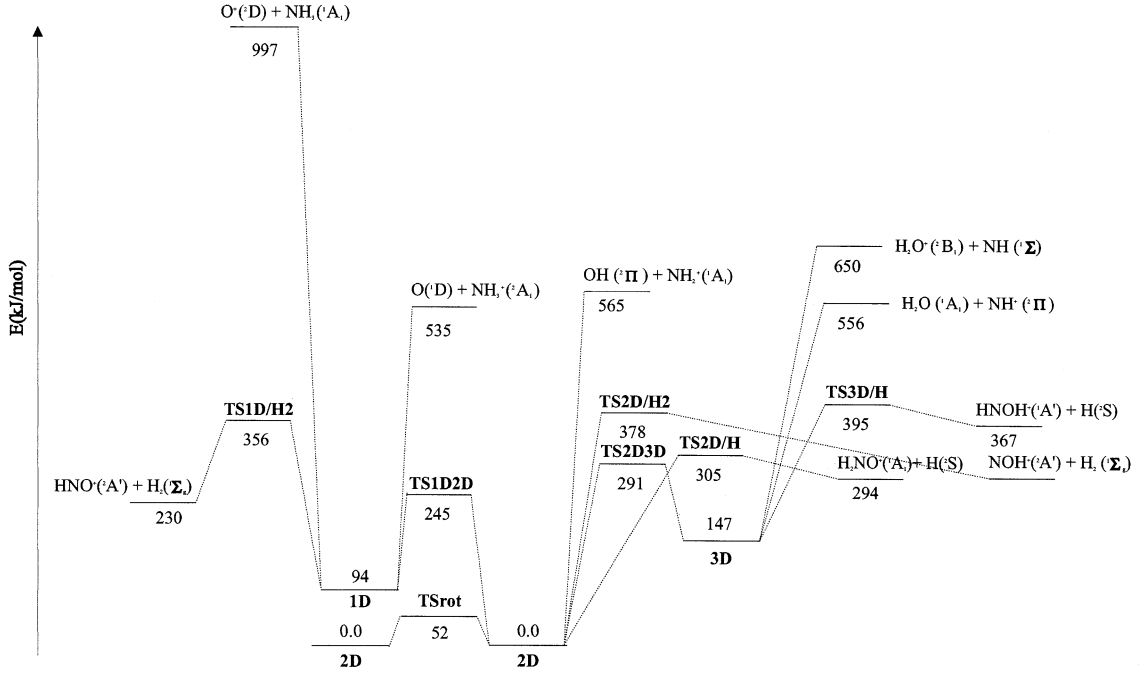

Fig. 2. Energy profile for the $[H_3,N,O]^+$ doublet PES. Values obtained at the G2//QCI level. The relative energies of the transient species **TS2D/H** and **TS3D/H** were obtained at the CCSD(T)/6-311+G(3df,2p)//QCISD/6-31+G(df,p) level (see text).

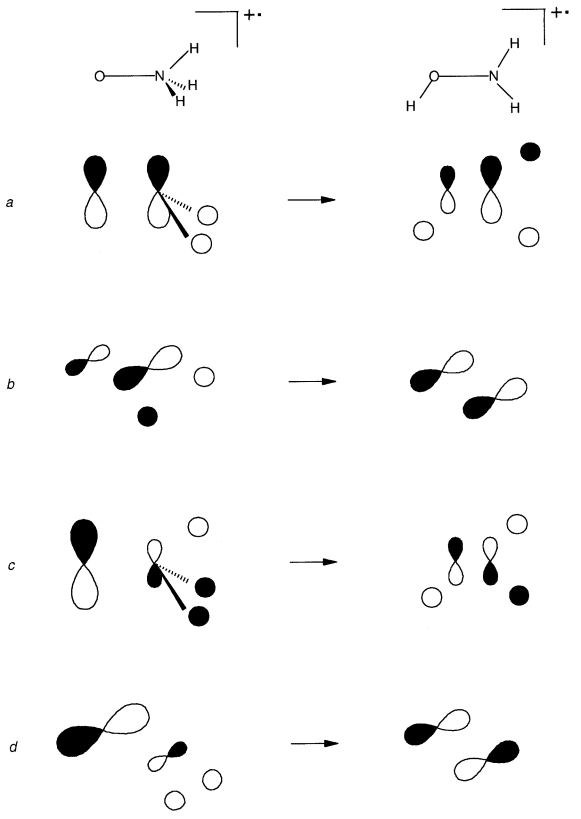

Fig. 3. Schematic representation of the π-type MOs of species **1D** (in the left of the figure) and **2D** (in the right of the figure).

N–O bond becomes sizably reinforced. Structure **2D** is consistently estimated to be about 94 kJ/mol more stable than species **1D**.

There is another important consequence which can be envisaged if one takes into account that species **2D** can be considered, alternatively, the result of removing one electron from hydroxylamine. In other words, hydroxylamine will have an electron configuration similar to that of species **2D** but with the *d* HOMO doubly occupied. Because, as mentioned above, this π orbital is N–O antibonding, the N–O linkage in neutral hydroxylamine should be a pure σ-bond, and therefore weaker than in its doublet-state cation. To ratify this from a more quantitative point of view, we have optimized the structure of neutral hydroxylamine at the same level of accuracy used to obtain the optimized geometries of the different cationic species investigated in this paper. These calculations show

Table 3
MP2/6-31G* harmonic vibrational frequencies (in cm^{-1}) for hydroxylamine and its cation **2D**

	2D	**Hydroxylamine**
NH_2 Pyramidalization	269	
N–O torsion	744	416
NOH and HNO asym. bending	1212	1453
NOH and HNO sym. bending	1468	1212
N–O stretch	1538	959
HNH bending		1729
N–H_2 sym. stretch	3490	3475
O–H stretch	3555	3785
N–H_2 asym. stretch	3666	3583

that indeed the N–O distance in neutral hydroxylamine is 0.13 Å longer than in species **2D**, whereas the charge density and the energy density at the corresponding bond critical point (see Table 2) are smaller in absolute value. As shown before in the literature [24], hydroxylamine is not planar, and the NH_2 group exhibits a significant degree of pyramidalization. This change in the bonding of hydroxylamine upon ionization is also mirrored in dramatic shiftings of the harmonic vibrational frequencies. As shown in Table 3, upon ionization both the N–O stretch and the torsion vibrational modes are shifted to higher frequencies; the former by more than 550 cm^{-1} and the latter by more than 300 cm^{-1}. The significant blue shift undergone by the torsion vibrational mode indicates that the rotational barrier around the N–O linkage must be smaller in the neutral than in the cation, where the N–O bond has a partial π-character. Because the rotational barrier of neutral hydroxylamine has been the object of many theoretical studies [25], we have considered it of interest to specifically investigate how this barrier changes upon ionization. For this purpose we have optimized the corresponding transition state (**TSrot**) at the same level of accuracy employed for the remaining species. Its optimized geometry has also been included in Fig. 1 and the corresponding G2//QCI energy in Table 1. From these values we can estimate a rotational barrier for species **2D** of 54 kJ/mol which is about 17 kJ/mol higher than the most accurate one reported in the literature [26] for the corresponding neutral species. The ionization potential of hydroxylamine estimated using our ap-

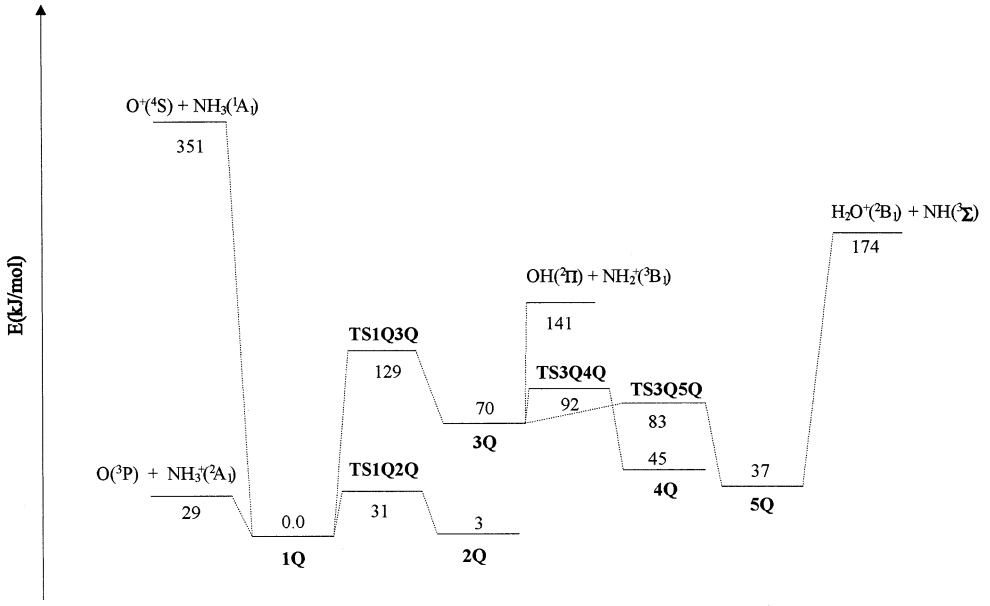

Fig. 4. Energy profile for the $[H_3,N,O]^+$ quartet PES. Values obtained at the G2//QCI level.

proach (9.3 eV) is in fairly good agreement with the available experimental values (10.0 and 9.6 eV) [27,28].

The global minimum, **2D**, evolves, through the transition state **TS2D3D**, which implies a further 1,2H shift, to yield the third local minimum of the PES, namely **3D**, which has a much weaker N–O bond (see Fig. 1 and Table 2). In this case the hydrogen shifting results in a large increase of the intrinsic electronegativity of the tricoordinated oxygen atom. As a consequence, the participation of the oxygen orbitals in the *b* π-orbital increases significantly and this MO becomes practically an oxygen lone pair. By orthogonality, the corresponding antibonding combination (*d* π-orbital) becomes a nitrogen lone pair. This implies that the N–O linkage has no π-character and becomes weaker. Accordingly, the charge density at the N–O bond critical point decreases (see Table 2) and structure **3D** has the smallest N–O stretching frequency (920 cm^{-1}), followed by species **1D** (1036 cm^{-1}), whereas, as mentioned above, the largest one (1538 cm^{-1}) corresponds to the global minimum **2D**. The weakening of the NO linkage is responsible for the low stability of species **3D**, which lies about 147 kJ/mol above species **2D**. This picture is consistent with the distonic character of structure **3D**, where the unpaired electron is located at the nitrogen atom, although the positive charge is associated with the OH_2 moiety.

3.3. $[H_3,N,O]^+$ quartet potential energy surface

The quartet PES is given schematically in Fig. 4. Contrary to what was found for doublet-state cations, the global minimum of this PES, **1Q**, can be viewed as a complex between an oxygen atom in its ^3P ground state and $NH_3^+(^2A_1)$. The corresponding spin densities corroborate that two unpaired electrons are associated with the O atom, whereas the third one is located in the NH_3 moiety, which also supports the positive charge. This implies that in the interaction between $O^+(^4S)$ and ammonia, the primary mechanism is a charge transfer process from the latter to the former. However, contrary to what happens in doublet-state cations, no standard covalent interactions are possible between $O(^3P)$ and $NH_3^+(^2A_1)$. The for-

Table 4
G2//QCI energies (in hartrees) of the possible products of the reactions of $O^+(^4S)$ and $O^+(^2D)$ with ammonia

$O(^1D)$	−74.905848
$O(^3P)$	−74.982030
$O^+(^2D)$	−74.355763
$O^+(^4S)$	−74.484971
$H_2O(^1A_1)$	−76.331931
$H_2O^+(^2B_1)$	−75.867842
$OH(^2\Pi)$	−75.643854
$NH_3(^1A_1)$	−56.457547
$NH_3^+(^2A_1)$	−56.083029
$NH_2^+(^3B_1)$	−55.378330
$NH_2^+(^1A_1)$	−55.333602
$NH(^3\Sigma)$	−55.141953
$NH(^1\Sigma)$	−55.077522
$NH^+(^2\Pi)$	−54.649118
$HNOH^+$	−130.552889
H_2NO^+	−130.580763
NOH^+	−129.914394
HNO^+	−129.938827
NO	−129.737162
NO^+	−129.402530
H_3^+	−1.323516

mation of a normal covalent bond, preserving the overall quartet multiplicity, would require the promotion of one electron from the highest occupied to the lowest unoccupied orbital of any of the interacting subunits, whose energetic cost is extremely high. Hence, the only possible interaction is the polarization of the oxygen atom by the NH_3^+ cation. In agreement with this picture, a NBO analysis of the corresponding wavefunction shows the existence of a N–O bonding singly occupied MO with a dominant contribution (82%) from an almost pure *p* orbital of the oxygen atom and a much smaller weight (18%) of the N *p* orbitals. Consistently, the interaction energy between both subunits is estimated to be only 29 kJ/mol, by using the G2//QCI energies given in Table 4. This weak N–O interaction makes the displacement of the oxygen atom around the NH_3^+ moiety not very demanding from the energetic point of view, and the PES shows a second local minimum, namely **2Q**, where the O atom is hydrogen bonded to the NH_3^+ subunit. Both minima are connected by a transition state, **TS1Q2Q**, which lies 31 kJ/mol above the global minimum.

A 1,2H shift through the transient species **TS1Q3Q**, yields the less stable local minimum, namely **3Q**. In this species the positive charge is associated with the NH_2 moiety so that this structure can be considered as an ion-dipole complex between $OH(^2\Pi)$ and $NH_2^+(^3B_1)$. A closer inspection of the wavefunction reveals that there is also a dative bond from the former to the latter. In fact the spin density of the NH_2^+ subunit is smaller (1.74) than what should be expected for a triplet-state cation, whereas that of the OH subunit (1.35) is larger than what should be expected for a doublet-state species. An NBO analysis of the wavefunction shows that there is indeed a N–O bonding orbital occupied by one β electron, in which the participation of the oxygen orbitals amounts to 66%.

An internal rotation of the NH_2 subunit leads to a new conformer **4Q**, where the OH moiety is hydrogen bonded to the NH_2^+ cation. Because the structure of this complex changed significantly when imposing tight convergency criteria along the MP2 geometry optimization, we have also imposed tight convergency criteria when its geometry was refined at the QCISD/6-31+G(df,p) level. The final geometry obtained (see Fig. 1) shows that the ionic hydrogen bond is quite strong, and the proton lies almost midway between both basic centers. This is reflected in an enhanced stability of the complex which lies almost 25 kJ/mol below its conformer **3Q**.

Species **5Q** can be obtained from structure **3Q** through a 1,2H shift that involves the **TS3Q5Q** transient species. In this isomer the positive charge is located on the OH_2 moiety, and the corresponding local minimum can be viewed as a tightly bound ion-dipole complex between $NH(^3\Sigma)$ and $H_2O^+(^2B_1)$. As in the previous cases, the interaction implies a strong polarization of the neutral, which is reflected in the formation of a singly occupied N–O bonding orbital, to which the nitrogen orbitals contribute 55%. Consistently, in this system, the spin density at the oxygen atom is only 0.57, whereas that at the nitrogen atom amounts to 2.41.

The relative stabilities of these complexes can be rationalized in terms of the electrostatic and polarization interactions between their building subunits.

From the values given in Table 4 it can be easily deduced that the interaction between $H_2O^+(^2B_1)$ and $NH(^3\Sigma)$ to yield species **5Q** (211.3 kJ/mol) is much stronger than that between $NH_2^+(^3B_1)$ and $OH(^2\Pi)$ (71.5 kJ/mol) to yield **3Q** local minimum, whereas the weakest interaction (28.9 kJ/mol) is that between $O(^3P)$ and $NH_3^+(^2A_1)$ to yield the global minimum **1Q**. In the first two cases, the dominant term arises from an ion-dipole interaction, which is absent in the latter case, explaining its low interaction energy. Hence, the large stability of the global minimum **1Q** simply reflects the large stability of $O(^3P)$ + $NH_3^+(^2A_1)$ with respect to $OH(^2\Pi)$ + $NH_2^+(^3B_1)$ and with respect to $H_2O^+(^2B_1)$ + $NH(^3\Sigma)$, rather than a strong interaction energy between the two building subunits.

If one takes into account that the dipole moments of $OH(^2\Pi)$ and $NH(^3\Sigma)$ are not significantly different (1.9 and 1.8 D, respectively), one must conclude that the significant differences between the stabilities of **3Q** and **5Q** local minima must arise from differences in the corresponding polarization terms. Assuming that the differences between the polarizabilities of NH and OH must be small, the polarization interactions must reflect both the ability of the electron donor (the neutral) to release electrons and the electron affinity of the electron acceptor. In other words, the greater these interactions, the smaller the ionization potential of the electron donor and the greater the electron affinity of the electron acceptor. This is indeed the case in complexes **3Q** and **5Q**. The $H_2O^+(^2B_1)$ species has an electron affinity (12.6 eV) sizably larger than that of $NH_2^+(^3B_1)$ (11.1 eV), while the ionization potential of $NH(^3\Sigma)$ (13.4 eV) is much smaller than that of $OH(^2\Pi)$ (15.4 eV).

The aforementioned trends in the interaction energies are also nicely reflected in the charge densities and energy densities evaluated at the corresponding N–O bond critical points (see Table 2). Similarly, the N–O stretching frequencies follow these trends. The smallest value (172 cm^{-1}) corresponds to the global minimum **1Q**, the largest one (625 cm^{-1}) corresponds to species **5Q**, although that of species **3Q** (542 cm^{-1}) is slightly smaller.

3.4. Reaction products

Since (as illustrated in Fig. 4) all activation barriers are much larger than the energy required for the dissociation of the global minimum, **1Q**, into $O(^3P)$ and $NH_3^+(^2A_1)$, one must conclude that the charge transfer process must be the most favorable mechanism in the gas-phase reactions between $O^+(^4S)$ and ammonia, in agreement with the experimental evidence [29]. According to our G2//QCI estimations this process is quite exothermic:

$$O^+(^4S) + NH_3 \rightarrow O(^3P) + NH_3^+(^2A_1)$$

$$\Delta H_0^0 = -322 \text{ kJ/mol} \quad (1)$$

The enthalpy of this reaction calculated using the experimental heat of the species involved [30] (334 kJ/mol) is in reasonably good agreement with our theoretical estimate.

For reactions involving the O^+ cation in its first ^2D excited state the situation is completely different. As shown in Fig. 2, the charge transfer process would involve the dissociation of **1D** into $O(^1D)$ + $NH_3^+(^2A_1)$ which requires an energy sizably larger than the isomerization barriers through the transient species **TS1D2D** and **TS2D3D**. Hence, in principle, the most favorable processes would be the formation of species **2D** and **3D**. The NO bond fission of these isomers would yield $OH(^2\Pi)$ + $NH_2^+(^1A_1)$ and $H_2O(^1A_1)$ + $NH^+(^2\Pi)$, respectively. Since the first ^2D excited state of O^+ lies about 318 kJ/mol above the ground state ^4S (see Table 4), these two processes are extremely exothermic:

$$O^+(^2D) + NH_3(^1A_1) \rightarrow OH(^2\Pi) + NH_2^+(^1A_1)$$

$$\Delta H = -431 \text{ kJ/mol} \quad (2)$$

$$O^+(^2D) + NH_3(^1A_1) \rightarrow H_2O(^1A_1) + NH^+(^2\Pi)$$

$$\Delta H = -440 \text{ kJ/mol} \quad (3)$$

The local minimum **3D** may also eventually dissociate into H_2O^+ $(^2B_1)$ + $NH(^1\Sigma)$:

$$O^+(^2D) + NH_3(^1A_1) \rightarrow H_2O^+(^2B_1) + NH(^1\Sigma)$$

$$\Delta H = -347 \text{ kJ/mol} \quad (4)$$

Table 5
Threshold energies (in eV) for the photodissociative ionization reactions of hydroxylamine

Reaction products	G2//QCI calculated value	Experimental value[a]
$HNO^+ + H_2$	11.65	11.56 ± 0.06
$NOH^+ + H_2$	12.31	12.34 ± 0.03
$HNOH^+ + H$	13.07	
$H_2NO^+ + H$	12.32	12.39 ± 0.01
$NH_2^+ + OH$	13.91	13.98 ± 0.03
$NH_3^+ + O$	12.74	12.70 ± 0.03

[a]Values taken from [28].

It is also worth noting that all these processes are accessible since all the stationary points of the PES are below the entrance channel in energy.

Other possible products can be the result of the dehydrogenation of the global minimum **2D**, which as we have mentioned above, is the ionized hydroxylamine. The G2//QCI total energies for these possible product ions, namely, HNO^+, NOH^+, $HNOH^+$, H_2NO^+ are given in Table 4.

Our results are consistent with the fact that two distinct thresholds were observed for formation of HNO^+ and NOH^+ in the photoionization mass spectrometry of hydroxylamine [28], associated with reactions (5) and (6).

$$H_2NOH + h\nu \rightarrow HNO^+ + H_2 + e^- \quad (5)$$

$$H_2NOH + h\nu \rightarrow NOH^+ + H_2 + e^- \quad (6)$$

Furthermore, as shown in Table 5, our estimates for the corresponding threshold energies are in very good agreement with the experimental values.

The experimental energy threshold for the removal of one H atom was reported to be 12.39 eV. From the experiment there is no way of knowing whether the product ion is $HNOH^+$ or H_2NO^+. Our results predict for the first reaction an energy threshold almost 1 eV higher than the experimental value, while for the second process our theoretical estimate agrees very well with the experimental outcome. Hence, we may conclude that, as described in Ref. [28], the major ion product formed in this reaction should be H_2NO^+. It is worth noting that (also in agreement with the experimental evidence) our results predict the same threshold energy for the formation of NOH^+ and H_2NO^+. The threshold energies for the photodissocative ionization reactions yielding NH_3^+ and NH_2^+ are also in good agreement with experimental values (see Table 5). Also important, the formation of these product ions in $O^+(^2D)$ reactions with ammonia are predicted to be extremely exothermic:

$$O^+(^2D) + NH_3 \rightarrow HNOH^+ + H, \quad \Delta H = -629 \text{ kJ/mol} \quad (7)$$

$$O^+(^2D) + NH_3 \rightarrow H_2NO^+ + H, \quad \Delta H = -702 \text{ kJ/mol} \quad (8)$$

$$O^+(^2D) + NH_3 \rightarrow HNO^+ + H_2, \quad \Delta H = -766 \text{ kJ/mol} \quad (9)$$

$$O^+(^2D) + NH_3 \rightarrow NOH^+ + H_2, \quad \Delta H = -702 \text{ kJ/mol} \quad (10)$$

We have also considered it of interest to investigate the mechanisms associated with these unimolecular dehydrogenations. For this purpose we have tried to locate the corresponding transition states at the same level of accuracy used for the remaining species included in this study. The loss of H_2 from the global minimum **2D** leads to the formation of $NOH^+(^2A')$ (see Fig. 2), through the transient species **TS2D/H2** (see Fig. 1). However, we could not find any direct pathway leading from the global minimum to $HNO^+(^2A') + H_2$. The mechanism proposed (see Fig. 2) implies as a first step the **2D-1D** isomerization, and then the loss of H_2 from **1D** through the transition state **TS1D/H2**. This is consistent with the conclusions of Kutina et al. [28], in the sense that the reaction pathway to NOH^+ from H_2NOH^+ should encounter much less steric hindrance than that toward HNO^+, even though the latter is favored energetically. The direct loss of H from the global minimum leads to the formation of $H_2NO^+(^1A_1)$(see Fig. 2) through the transition state **TS2D/H** (see Fig. 1).

The corresponding pathway leading to $HNOH^+$

(see Fig. 2) implies a **2D-3D** isomerization, as a first step, followed by a H loss through the transient species **TS3D/H** (see Fig. 1). Since, as mentioned above, these two transient species (**TS2D/H**, **TS3D/H**) have a non-negligible spin contamination, the corresponding activation barriers were estimated using a CCSD(T) formalism which has been shown [11] to be reliable to treat radicals with high spin contamination. The basis set expansion used was 6-311+G(3df,2p). Nevertheless the barriers so obtained are identical to those calculated at the G2//QCI level (see Table 1).

The mechanisms associated with the unimolecular dehydrogenation processes of $[H_2,N,O]^+$ species to yield NO^+ were reported before in the literature [31] at similar levels of theory, and they will not be included here.

From the estimated activation barriers corresponding to the loss of H_2 (either to yield NOH^+ or HNO^+, and the loss of H to yield H_2NO^+ and $HNOH^+$) we can conclude that all these processes are more favorable than the charge transfer yielding NH_3^+. Hence, in contrast with the $O^+(^4S)$ reactions with ammonia, in the $O^+(^2D)$ reactions the major products should be H_2NO^+, NOH^+, HNO^+ and $HNOH^+$, whereas NH_3^+, NH^+ and NH_2^+ should be minor products.

We have also considered it of interest to investigate whether the formation of these ions (in particular NOH^+, HNO^+, and H_2NO^+) in H_3^+ reactions with NO are exothermic processes. In fact, reactions (11)–(13) were proposed by Loew et al. [32] as possible depletion mechanisms for NO in dense interstellar clouds, to explain why NO had not been detected, at that time, even though it should be a major component of these clouds.

From the G2//QCI energy of H_3^+ given in Table 4 it can be concluded that all three processes should be exothermic, in agreement with the previous estimates of Kutina et al. [28] based in their own estimations for the heat of formation of NOH^+, HNO^+, and H_2NO^+ species.

$$H_3^+ + NO \rightarrow NOH^+ + H_2$$

$$\Delta H = -53 \text{ kJ/mol} \quad (11)$$

$$H_3^+ + NO \rightarrow HNO^+ + H_2$$

$$\Delta H = -117 \text{ kJ/mol} \quad (12)$$

$$H_3^+ + NO \rightarrow H_2NO^+ + H$$

$$\Delta H = -53 \text{ kJ/mol} \quad (13)$$

Also, interestingly, the formation of $HNOH^+$ is predicted to be endothermic:

$$H_3^+ + NO \rightarrow HNOH^+ + H$$

$$\Delta H = +20 \text{ kJ/mol} \quad (14)$$

and therefore this reactive channel should not contribute to the depletion of NO.

4. Conclusions

We have explored the most outstanding features of the $[H_3,N,O]^+$ doublet- and quartet-state PESs to gain some insight on the possible reaction mechanisms involved in $O^+(^4S)$ and $O^+(^2D)$ reactions with ammonia. However, in the present approach no attempt was made to account for possible crossings between both PESs. Our results show that the bonding characteristics of $[H_3,N,O]^+$ doublet- and quartet-state cations are rather different. The latter are weakly bound species involving one-electron linkages, whereas the former present normal covalent bonds. The global minimum of the doublet PES is the $HONH_2^+$ **2D** species, which has a N–O linkage with a partial double-bond character. This means that the ionization of hydroxylamine implies an important enhancement of the stability of the N–O bond, which upon ionization becomes much shorter, although its stretching frequency is significantly blue-shifted. Consistently, the rotational barrier in the cation is also larger than in the neutral species. For the quartets the global minimum can be viewed roughly as the interaction between O in its ^3P ground state and $NH_3^+(^2A_1)$, reflecting the large electron recombination energy of $O^+(^4S)$ which strongly favors the charge transfer process from the ammonia molecule.

From the characteristics of both $[H_3,N,O]^+$ dou-

blet- and quartet-state PESs we may conclude that the products of both reactions are significantly different. For reactions involving O^+ in its ^4S ground state, only the charge transfer process should be observed, in agreement with the experimental evidence [29]. In reactions involving O^+ in its ^2D first excited state, the charge transfer process is energetically disfavored with respect to the dehydrogenation mechanisms. Hence, the major reaction products should be H_2NO^+, HNO^+, NOH^+, $HNOH^+$, although NH_3^+, NH^+ and NH_2^+ should be minor products. All these processes are predicted to be exothermic.

We can also conclude that the reactions between H_3^+ and NO to yield either NOH^+, HNO^+, or H_2NO^+ are exothermic processes and therefore they can be responsible for the depletion of NO in the dense interstellar clouds.

In general, the most outstanding features of the $[H_3,N,O]^+$ doublet- and quartet-state PESs closely resemble those reported before [9] for the $[H_2,O_2]^+$ PESs.

Acknowledgements

This work has been partially supported by the DGES Project No. PB96-0067. A.I.G. gratefully acknowledges a grant from the Ministerio de Educación y Cultura of Spain. We thank one of our reviewers for helpful criticism.

References

[1] See for instance (a) C.E.A. Hop, H. Chen, P.J.A. Ruttink, J.L. Holmes, Org. Mass. Spectrom., 26 (1991) 679. (b) D.K. Bohme, Chem. Rev. 92 (1992) 1487. (c) S.G. Lias, J.E. Bartmess, J.F. Liebman, J.L. Holmes, R.D. Levin, W.G. Mallard, J. Phys. Chem. Ref. Data 17 (1988) 1(suppl).
[2] F. Cacace, M. Speranza, Science 265 (1994) 208.
[3] F. Cacace, Pure Appl. Chem, 69(2) (1997) 227.
[4] A. Luna, O. Mó, M. Yáñez, J. Mol. Struct. (Theochem) 310 (1994) 135.
[5] A. Luna, M. Yáñez, J. Phys. Chem. 97 (1993) 10659.
[6] A.I. González, M. Yáñez, Chem. Phys. Lett. 248 (1996) 102.
[7] A. Luna, M. Manuel, O. Mó, M. Yáñez, J. Phys. Chem. 98 (1994) 6980.
[8] M. Manuel, O. Mó, M. Yáñez, J. Phys. Chem. 101 (1997) 1722.
[9] A.I. González, O. Mó, M. Yáñez, Anales de Química (Int. Ed.), 93 (1997) 310.
[10] J.A. Pople, M. Head-Gordon, K. Raghavachari, J. Chem. Phys. 87 (1987) 5968.
[11] P.M. Mayer, C.J. Parkinson, D.M. Smith, L. Radom, J. Chem. Phys. 108 (1998) 604.
[12] F. Angelelli, M. Aschi, F. Cacace, F. Pepi, G. Depetris, J. Phys. Chem. 99 (1995) 6551.
[13] M. Esseffar, A. Luna, O. Mó, M. Yáñez, J. Phys. Chem. 97 (1993) 6607.
[14] M.J. Frisch, G.W. Trucks, H.B. Schlegel, P.M.W. Gill, B.G. Johnson, M.A. Robb, J.R. Cheeseman, T.A. Keith, G.A. Petersson, J.A. Montgomery, K. Raghavachari, L.A. Al-Laham, V.G. Zakrzewski, J.V. Ortiz, J.B. Foresman, J. Cioslowski, B.B. Stefanow, A. Nanayaklara, M. Challacombe, C.Y. Peng, P.Y. Ayala, W. Chen, M.W. Wong, J.L. Andres, E.S. Replogle, R. Gomperts, R.L. Martin, D.J. Fox, J.S. Binkley, D.J. Defrees, J. Baker, J.P. Stewart, M. Head-Gordon, C. Gonzalez, J.A. Pople GAUSSIAN 94, Revision D.1, Gaussian, Inc., Pittsburgh, PA, 1995.
[15] L.A. Curtiss, K. Raghavachari, G.W. Trucks, J.A. Pople, J. Chem. Phys. 94 (1991) 7221.
[16] (a) G.A. Petersson, T.G. Tensfeldt, J.A. Montgomery Jr., J. Chem. Phys. 94 (1991) 6091. (b) J.A. Montgomery Jr., J.W. Ochterski, G.A. Petersson, J. Chem. Phys. 101 (1994) 5900.
[17] J.A. Pople, A.P. Scott, M.W. Wong, L. Radom, Isr. J. Chem., 33 (1993) 345.
[18] F. Weinhold, J.E. Carpenter, The Structure of Small Molecules and Ions, Plenum, NY, 1988.
[19] (a) R.F.W. Bader, H. Essén, J. Chem. Phys. 80 (1984) 1943. (b) R.F.W. Bader, P.J. MacDougall, C.D. Lau, J. Am. Chem. Soc. 106 (1984) 1594. (c) R.F.W. Bader, Atoms in Molecules. A Quantum Theory, Oxford University Press, New York, 1990.
[20] D. Cremer, E. Kraka, Angew. Chem. 96 (1984) 612.
[21] The AIMPAC programs package has been provided by J. Cheeseman and R.F.W. Bader.
[22] K. Raghavachari, J.B. Anderson, J. Phys. Chem. 100 (1996) 12960.
[23] W.L. Wiese, M.W. Smith, B.M. Glennon, National Standard Reference Data Series (NBS4) 1, 1966.
[24] L.A. Curtiss, J. Chem. Phys. 77 (1982) 3605.
[25] See, for instance, P.W. Payne, L.C. Allen, in Applications of Electronic Structure Theory, H.F. Schaefer III (Ed.), Plenum, New York, 1977, and references therein.
[26] A. Chung-Phillips, K.A. Jebber, J. Chem. Phys. 102 (1995) 7080.
[27] I.A. Koppel, U.H. Molder, R.J. Pikver, Org. React. Tartu. 20 (1983) 45.
[28] R.E. Kutina, G.L. Goodman, J. Berkowitz, J. Chem. Phys. 77 (1982) 1644.
[29] (a) N.G. Adams, D. Smith, J.F. Paulson, Chem. Phys. 72 (1980) 288; (b) D. Smith, N.G. Adams, T.M. Miller, J. Chem. Phys. 69 (1978) 308.
[30] S.G. Lias, J.E. Bartmess, J.F. Liebman, J.L. Holmes, R.D. Levin, W.G. Mallard, J. Phys. Chem. Ref. Data 17 (1988) 1 (suppl).
[31] D. Schröder, F. Grandinetti, J. Hrusák, H. Schwarz, J. Phys. Chem. 96 (1992) 4841.
[32] G.H. Loew, D.S. Berkowitz, S. Chang, Astrophys. 219 (1978) 458.